Heliyon 10 (2024) e40429

Contents lists available at ScienceDirect

Heliyon

journal homepage: www.cell.com/heliyon

Research article

Optimized co-delivery of curcumin and methylprednisolone using polyvinyl alcohol-coated CuO nanoparticles for synergistic rheumatoid arthritis treatment

Kimiya Zarei [a], Mehdi Jahanbakhshi [b,*], Reza Nahavandi [b], Reza Emadi [c]

[a] Faculty of Pharmacy and Pharmaceutical Sciences, Tehran Medical Sciences, Islamic Azad University, Tehran, 1916893813, Iran
[b] School of Chemical Engineering, College of Engineering, University of Tehran, Tehran, Iran
[c] Department of Biochemistry, Institute of Biochemistry & Biophsysics (IBB), University of Tehran, Tehran, Iran

ARTICLE INFO

Keywords:
Co-delivery
Curcumin
Methylprednisolone
Polyvinyl alcohol
Rheumatoid arthritis

ABSTRACT

The combination of methylprednisolone (MPDL) and curcumin (CUR) for treating rheumatoid arthritis (RA) offers several therapeutic advantages. This synergy allows for a reduction in the dosage of methylprednisolone, minimizing potential side effects associated with long-term steroid use while maintaining or enhancing the treatment's effectiveness. The objective of this study is to prepare drug carriers for MPDL and CUR aimed at treating RA, utilizing Freund's Complete Adjuvant-induced arthritic rat model (AIA). CuO nanoparticles (NPs) were synthesized using ultrasound by reducing copper (II) sulfte pentahydrate with sodium borohydride in a basic solution. Subsequently, these nanoparticles were incrementally added to a polyvinyl alcohol (PVA) solution to ensure controlled integration of PVA-coated CuO NPs. Field Emission Scanning Electron Microscopy (FE-SEM) analysis revealed that the CuO nanoparticles and PVA-coated CuO NPs averaged sizes of 50.7 nm and 104.8 nm, respectively. Furthermore, the PVA-coated CuO NPs demonstrated remarkable biocompatibility, with cell viability ranging from 88.1 % to 92.1 % at concentrations of 0.1 μg/mL and 50 μg/mL after 72 h, as validated through the MTT assay. The PVA-coated CuO NPs exhibited a more controlled and gradual drug release profile for both CUR and MPDL when compared to the PVA matrix. CUR@MPDL@PVA-coated CuO NPs demonstrated the most substantial reduction in hind paw swelling and the minimal clinical scores among all treatment groups, signaling enhanced anti-inflammatory effects. CUR@MPDL@PVA-coated CuO NPs also notably reduced the concentrations of pro-inflammatory cytokines TNF-α and IL-1β when measured against the AIA rats and the groups treated with free agents. Therefore, CUR@MPDL@PVA-coated CuO nanoparticles can be used in biomedical applications due to their size, biocompatibility, and anti-inflammatory properties.

1. Introduction

Rheumatoid arthritis (RA) represents a persistent autoimmune disorder characterized by chronic synovial inflammation, leading to progressive joint deterioration, pain, and a detrimental impact on the quality of life [1]. Despite substantial strides in comprehending RA's pathophysiology, its management remains a formidable challenge, necessitating innovative therapeutic approaches. Current

* Corresponding author. University of Tehran, Tehran, Iran.
E-mail address: m.jahanbakhshi@ut.ac.ir (M. Jahanbakhshi).

https://doi.org/10.1016/j.heliyon.2024.e40429
Received 11 July 2024; Received in revised form 11 November 2024; Accepted 13 November 2024
Available online 15 November 2024

treatment strategies predominantly rely on Disease-modifying anti-rheumatic drugs (DMARDs) and glucocorticoids, with methotrexate (MTX) and methylprednisolone (MPDL) serving as prominent examples in each category [2]. These agents aim to alleviate symptoms, decelerate disease progression, and enhance the patient's well-being [3]. However, systemic side effects and variability of responses among patients limit the efficacy of current therapies, highlighting the need for innovative and more effective therapeutic approaches [4,5].

Copper nanoparticles (Cu NPs) have emerged as a versatile and biocompatible platform for drug delivery applications [6]. Their unique physicochemical properties make them well-suited for encapsulating and delivering therapeutic agents to specific target sites, such as inflamed synovial joints in RA. Cu nanoparticles offer several advantages in drug delivery [7,8]. Cu is a vital trace element within the human body, playing a crucial role in ensuring the compatibility of copper nanoparticles [9]. Also, Cu nanoparticles can be modified to control their surface properties, allowing for precise control over drug release rates and targeting specificity [10]. Cu nanoparticles can sustain drug release over extended periods, ensuring a prolonged therapeutic effect [11]. Furthermore, the localized delivery of therapeutics using Cu nanoparticles reduces systemic toxicity, a critical consideration in RA therapy [12].

Polyvinyl alcohol (PVA), a biocompatible and stable material, is a preferred choice for hydrogel formulations [13]. PVA versatility arises from the availability of hydroxyl (OH) groups along its polymer chains, allowing it to form cross-linked structures through various physical and chemical methods [14,15]. In biomedical applications, PVA hydrogels have emerged as an attractive option for contact lenses, artificial heart linings, wound dressings, drug delivery systems, and even artificial cartilage for orthopedic surgery [16,17]. Due to their high levels of biocompatibility, transparency, nontoxicity, and lack of carcinogenicity, they have many potential medical applications that advance patient care and satisfaction [18,19].

This research endeavors to address the complexities of RA treatment by pioneering a novel nanomedicine approach. Specifically, this study explores the co-delivery of MPDL, a potent glucocorticoid, and curcumin (CUR), a natural anti-inflammatory compound, utilizing copper nanoparticles as an ideal drug delivery platform [20]. The choice of MPDL and CUR as therapeutic agents is grounded in their well-established mechanisms of action, which collectively target pivotal pathways implicated in RA pathogenesis, including regulating inflammation, immune responses, and oxidative stress [21]. Due to their pharmacokinetic characteristics, MPDL and CUR present a number of significant challenges in clinical settings that restrict their potential as therapeutic agents. Curcumin has strong anti-inflammatory and antioxidant effects, but its low solubility, quick metabolism, and restricted tissue distribution make it poorly bioavailable. The clinical efficacy of curcumin is lowered as a result of insufficient concentrations of the drug reaching the target tissues. On the other hand, methylprednisolone is a synthetic glucocorticoid that is frequently used due to its potent immunosuppressive and anti-inflammatory properties. However, its long-term use is associated with significant systemic side effects, such as osteoporosis, weight gain, hypertension, and immunosuppression, which limit its utility in chronic treatment regimens. The formulation of PVA-coated CuO nanoparticles is specifically designed to address these challenges by improving the delivery and efficacy of both drugs. The encapsulation of curcumin within the PVA-coated CuO nanoparticles enhances its solubility and stability, protecting it from rapid metabolism and enabling a more controlled and sustained release. This targeted delivery system ensures higher concentrations of curcumin at the site of inflammation, improving its therapeutic impact while minimizing systemic exposure. For methylprednisolone, the nanoparticle formulation offers a means to reduce the dosage required for therapeutic effect, thereby mitigating the risk of systemic side effects. The PVA coating provides a biocompatible barrier that controls the release of methylprednisolone, allowing for more sustained and localized delivery to inflamed tissues. This reduces the need for frequent dosing and minimizes the systemic distribution of the drug, addressing the adverse effects typically associated with its prolonged use.

The co-delivery of methylprednisolone and curcumin within CuO nanoparticles represents a pioneering and multifaceted strategy to revolutionize the treatment landscape of RA. This research endeavors to unlock the full therapeutic potential of these agents, offering the promise of enhanced efficacy, reduced side effects, and improved patient outcomes. As we navigate the complex landscape of nanomedicine, precision drug delivery, and co-therapy strategies, our ultimate goal is to provide new hope for individuals grappling with the formidable challenges posed by RA.

2. Experimental

2.1. Materials

Polyvinyl alcohol (PVA), copper sulfate pentahydrate ($CuSO_4{\cdot}5H_2O$ (98 %)), sodium borohydride ($NaBH_4$ (99 %)), and cetyltrimethylammonium bromide (CTAB ($\geq$99 %)) were all purchased from Sigma Aldrich. Curcumin was procured from Merck in Germany, while methylprednisolone was obtained from Exir Pharmaceutical Company in Iran. Dialysis membranes with a Molecular Weight Cut-Off (MWCO) of 12,000–14,000 Da were sourced from SLS in the United Kingdom. Additionally, sodium phosphate, potassium phosphate, potassium chloride, and sodium chloride were acquired from Sigma in the USA.

2.2. Optimum synthesis method for CuO and PVA-coated CuO NPs

The synthesis of CuO nanoparticles in this study is achieved through a carefully optimized method involving the reduction of copper (II) sulfate pentahydrate salt ($CuSO_4{\cdot}5H_2O$) in the presence of sodium borohydride ($NaBH_4$) within a basic medium, facilitated by ultrasound waves. To stabilize the reaction, cetyltrimethylammonium bromide (CTAB), a cationic surfactant, is employed [22]. Initially, in a glass vial, 7.5 mL of NaOH (4.4 mM) and 7.5 mL of CTAB (16 mM) were combined and thoroughly mixed in an ultrasonic bath at a temperature of 30 °C for a duration of 5 min. Subsequently, 50 μL of $CuSO_4{\cdot}5H_2O$ (0.4 M) was introduced into the vial and subjected to mixing for another 5 min, yielding a copper hydroxide suspension displaying a light blue hue. A cold solution freshly

prepared at 100 μL of $NaBH_4$ (2 M) was then swiftly introduced, leading to a noticeable transformation from light blue to a deep brown hue. The reaction was maintained in the ultrasonic bath for a total of 15 min, following which the vial was sealed and stored at 23 °C. The CuO nanoparticles were considered formed when the colloidal suspension transitioned to a yellow coloration. The synthesis of PVA-coated CuO NPs involved a meticulously executed procedure. Initially, a PVA solution was prepared with precise concentrations, ensuring the desired viscosity and stability. Subsequently, the CuO NPs were introduced drop by drop into the PVA solution under controlled conditions, allowing for a gradual and controlled incorporation of the nanoparticles. Scheme 1 shows the schematic synthesis of PVA-coated CuO NPs and their interaction with drugs.

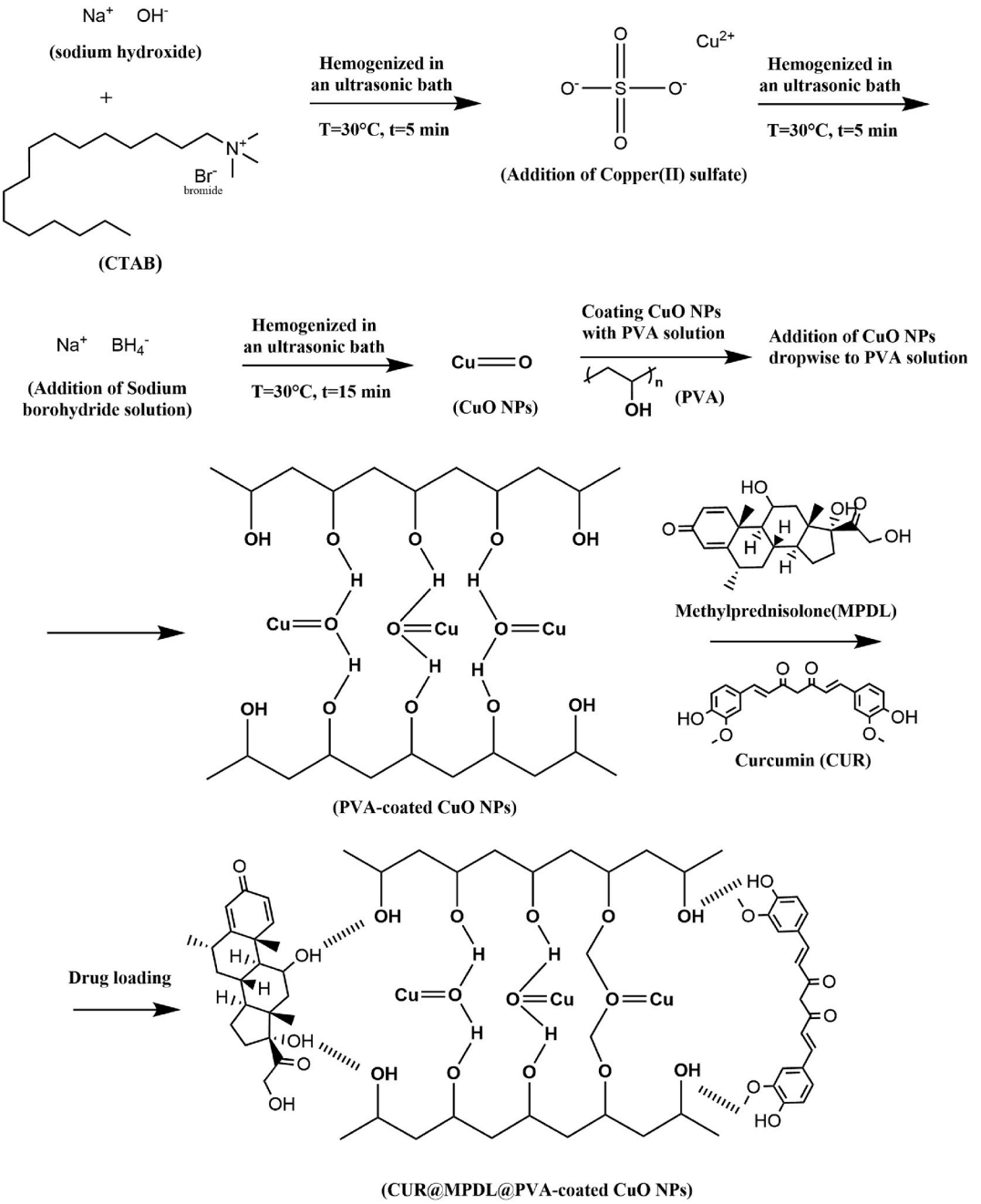

Scheme 1. Schematic synthesis of PVA-coated CuO NPs and their interaction with drugs.

2.3. Characterization

FTIR spectra of the nanoparticles were obtained using an Agilent Cary 630 FTIR spectrometer without additional sample preparation. Surface morphology was examined via SEM using a Topcon instrument, with samples gold-coated to 16 nm thickness using a Bal-tec system (USA). AFM analysis, performed in contact mode, utilized a NanoScope E system by Digital Instruments (USA). Particle size, distribution, and zeta potential were measured using dynamic and electrophoretic light scattering by Malvern Instruments (UK). TGA was conducted with a Netzsch STA 449F3 Calorimeter (Germany) and a TGA 50 model (Japan) at a heating rate of 10 °C/min from 25 to 600 °C under nitrogen.

2.4. In vitro characterization of the delivery system

2.4.1. Drug loading procedure

In the drug loading procedure, curcumin and methylprednisolone were solubilized individually in appropriate solvents to formulate drug solutions of precise concentrations. Subsequently, a carefully measured volume of each drug solution was carefully introduced into the pre-prepared PVA-coated CuO NPs. Gentle agitation was conducted to promote the effective loading of curcumin and methylprednisolone onto the nanoparticle surface. Following the drug-loading process, the drug-loaded nanoparticles were separated from the reaction mixture by centrifugation. In subsequent separation steps, the synthesized nanoparticles were thoroughly washed to remove any unbound drug molecules. The purified drug-loaded nanoparticles were then dried in preparation for the following analyses and characterization. This careful drug loading technique ensured the accurate incorporation of curcumin and methylprednisolone onto the PVA-coated CuO NPs, facilitating further investigations into drug release and further assessment of their therapeutic capabilities.

2.4.2. Drug release study

To investigate drug release, the drug-loaded PVA-coated CuO NPs were completely suspended in phosphate-buffered saline (PBS), initiating the release study. Dialysis membranes with a molecular weight cut-off (MWCO) of 12,000–14,000 Da were strategically employed to facilitate the process. These specialized membranes facilitated the precise separation of the drug-loaded nanoparticles from the release medium, enabling optimal control over the drug release study. Under rigorously controlled conditions, the release study proceeded, involving periodic sampling of the release medium at predefined time intervals. To assess the efficacy and kinetics of drug release, the concentrations of methylprednisolone and curcumin released from PVA-coated CuO NPs and PVA matrix were quantified using well-established analytical techniques. Firstly, 2 mL of each sample was pipetted into a 12 kDa dialysis membrane and placed into 50 mL of PBS solution at pH = 7.4 at 37 °C with stirring. Each sample was put into the dialysis bag separately and sunk in a separate PBS solution. At predetermined time intervals, 1 mL of each release medium was withdrawn and replaced with an equal volume of fresh solution. Drug concentration was quantified using UV–visible spectroscopy (JASCO, V-530, Japan) at 425 nm for CUR and 247 nm for MPDL, respectively. Drug release profiles were plotted for different samples and analyzed using different kinetic models.

2.5. MTT assay

Human foreskin fibroblasts (HFF-1) were cultured under carefully controlled conditions. The cells were incubated in a cell incubator, maintaining an airflow containing 5 % CO_2 and the temperature set at 37 °C. The growth medium used for the culture was composed of DMEM (90 %), supplemented with FBS (10 %) and penicillin/streptomycin (1 %) to promote cell growth and proliferation. After reaching 80 % of confluency, the cells were removed by trypsin and subsequently suspended with PBS. Before their utilization in experiments, the viability of these cells was assessed by staining them with 0.1 % trypan blue and conducting a cell count under a microscope. For evaluating cell viability, the widely adopted MTT (3-(4,5-dimethylthiazol-2-yl)-2,5-diphenyltetrazolium bromide) assay was used. Initially, when the cells reached a confluence of approximately 80%–90 %, they were seeded into a 96-well plate, each well receiving a density of 1×10^5 cells. These cells were then allowed to incubate for a period of 24 h. After the 24-h incubation period. The cells were carefully detached from the medium and washed in PBS. Subsequently, test samples containing DMEM medium at varying concentrations (0.1–50 μg/mL) were introduced to the wells, and the cells were further incubated for an additional 48 and 72 h. Following this incubation period, the medium was once again removed, and the MTT assay was administered to the cells. The cells were incubated with the MTT solution for a duration of 4 h. After this incubation, the MTT solution was removed, and 100 μl of dimethyl sulfoxide (DMSO) was added to each well. An ELISA microplate reader set at a wavelength of 570 nm (ELx808i, BioTek Instruments, USA) was utilized to measure the absorbance. Cell viability percentages were calculated using the following formula (Equation (1)):

$$Cell\ viability = \frac{Absorbance\ of\ treated\ cells}{Absorbance\ of\ control\ cells} \times 100 \quad (1)$$

2.6. In vivo anti-arthritic effect

Male Sprague–Dawley rats were sourced from the Pasteur Institute of Iran. The induction of arthritis was carried out using the standard method for Complete Freund's Adjuvant (CFA) as outlined in previous studies [23]. The rats were injected subcutaneously

with 100 μL of CFA and housed under controlled environmental conditions with a 12-h light/dark cycle in polystyrene cages with wood shavings. They were provided with standard rodent food and water, which were freely available. The arthritic rats were then divided into four equal groups (four rats per group, n = 4), with the saline group serving as a control. The same quantities of therapeutics were loaded into nanoparticles. The treatment, which began on day 9 and continued every alternate day until day 28, aimed to assess therapeutic effectiveness. Paw swelling in the right hind paw was measured using a plethysmometer, and the experiments were conducted blindly. The therapeutic impact was also assessed based on a clinical scoring system ranging from 0 (normal) to 4 (severe swelling and widespread erythema). The treatment groups received CUR, MPDL, and CUR@MPDL@PVA-coated CuO NPs as follows: Model group: untreated arthritic rats were administered 3 mL/kg b.w. of saline solution, Cur group: arthritic rats treated with 15 mg/kg b.w. of curcumin (i.p.), Mlx group: arthritic rats treated with 4 mg/kg b.w. of meloxicam (i.p.), Cur/Mlx group: arthritic rats treated with 15 mg/kg b.w. of curcumin plus 4 mg/kg b.w. of meloxicam (i.p.), nCur group: arthritic rats treated with PLGA nanoparticles encapsulating 15 mg/kg b.w. of curcumin (i.p.), nMlx group: arthritic rats treated with PLGA nanoparticles encapsulating 4 mg/kg b.w. of meloxicam (i.p.), nCur/Mlx group: arthritic rats treated with PLGA nanoparticles co-encapsulating 15 mg/kg b.w. of curcumin plus 4 mg/kg b.w. of meloxicam (i.p.).

2.7. Statistical analysis

Based on at least three repetitions, all values were reported as the mean ± SD. GraphPad Prism 8 (GraphPAD Software Inc., USA) was used to create the graphs, and student's t-test and one-way ANOVA were used for statistical analysis. A statistically significant p-value was defined as less than 0.05. The graphs with asterisks denote statistical significance: * for $p \leq 0.05$, ** for $p \leq 0.01$, *** for $p \leq 0.001$, and **** for $p \leq 0.0001$.

3. Results

3.1. Optimization of PVA-coated CuO nanoparticles for drug delivery

Box-Behnken Design (BBD) for the response surface methodology (RSM) was used to enhance the performance of PVA-coated CuO NPs for drug delivery, focusing on the influence of three key factors: A:PVA: CuO ratio (Factor 1), Curcumin concentration (Factor 2), and Methylprednisolone concentration (Factor 3) (Table 1). The responses investigated included nanoparticle size (Response 1), EE of Methylprednisolone (Response 2), and EE of Curcumin (Response 3). The experimental runs, conducted according to the factorial design, resulted in varying responses, reflecting the influence of the different factors on the final results. Notably, Run 5, with a higher A:PVA: CuO ratio (2), increased curcumin concentration (5 mg), and higher methylprednisolone concentration (15 mg), exhibited the largest nanoparticle size (362.12 nm) and the highest encapsulation efficiencies for both methylprednisolone (85.055 %) and curcumin (67.059 %). The A:PVA: CuO ratio emerged as a critical factor affecting nanoparticle characteristics. Higher ratios (Runs 5 and 15) led to larger nanoparticles, while lower ratios (Run 13) resulted in smaller sizes. Interestingly, EE for both drugs showed an optimal range, with Run 8 having an A:PVA: CuO ratio of 1.5, exhibiting the highest encapsulation efficiencies for both methylprednisolone (81.545 %) and curcumin (59.754 %). Curcumin and methylprednisolone concentrations significantly influenced encapsulation efficiencies. Elevated drug concentrations (Runs 5, 8, and 15) generally enhanced EE, with Run 5 demonstrating the most favorable outcomes. Nanoparticle size demonstrated an inverse relationship with drug encapsulation efficiencies. Larger nanoparticles (Runs 5 and 15)

Table 1
Nanoparticle size, and EE% of Different PVA-coated CuO NPs containing curcumin and methylprednisolone. Data are represented as Mean ± SD, n = 3.

Std	Run	Factor 1	Factor 2	Factor 3	Response 1	Response 2	Response 3
		A:PVA: CuO	B: Curcumin	C: Methylprednisolone	Size	EE (methylprednisolone)	EE (curcumin)
		ratio	mg	mg	nm	%	%
17	1	1.5	5	12.5	260.96	74.062	71.166
14	2	1.5	5	12.5	264.3	74.458	72.305
16	3	1.5	5	12.5	262.47	75.551	70.641
9	4	1.5	3	10	219.21	68.704	54.444
8	5	2	5	15	362.12	85.055	67.059
2	6	2	3	12.5	333.37	77.112	52.951
7	7	1	5	15	215.28	83.241	68.715
12	8	1.5	7	15	275.82	81.545	59.754
3	9	1	7	12.5	201.56	74.321	60.512
6	10	2	5	10	304.11	68.871	71.081
15	11	1.5	5	12.5	258.32	75.149	74.335
11	12	1.5	3	15	255.21	85.488	55.132
1	13	1	3	12.5	196.71	72.644	51.285
13	14	1.5	5	12.5	262.84	77.021	70.608
4	15	2	7	12.5	382.1	73.548	61.025
5	16	1	5	10	185.49	67.659	73.352
10	17	1.5	7	10	232.62	66.215	60.987

exhibited higher EE values for both drugs, likely attributed to the increased surface area available for drug encapsulation. Considering the diverse responses, the optimal conditions for PVA-coated CuO NPs, balancing the size and drug encapsulation efficiencies, appear to be a ratio of 1.5 for A:PVA: CuO, a curcumin concentration of 5 mg, and a methylprednisolone concentration of 15 mg (Fig. 1).

3.2. Synthesis of CuO and PVA-coated CuO NPs

The choice of reducing agent plays a pivotal role in determining the success of copper nanomaterial synthesis. While various reducing agents are available, such as sodium citrate, reducing sugar, ascorbic acid, and hydrazine, $NaBH_4$ is selected here due to its robust reducing properties, as previously demonstrated (Fig. 2a) [22]. The process by which Cu^{2+} ions are depleted to Cu^0 or Cu^+ by $NaBH_4$ initiates the formation of Cu nanoparticles. The sonochemical method is the primary experimental condition adopted for the synthesis. Utilizing ultrasound waves serves to stimulate the development of various nanostructures of metal oxide by altering the shape of the micelles used as templates and expediting the rearrangement of reactions. Sonochemical synthesis has been well-established for efficiently producing CuO nanoparticles, yielding various morphologies, including spherical, rod-shaped, leaf-like, and amorphous structures. Incorporating CTAB into the synthesis process significantly influences the morphology of the CuO nanoparticles. Minor additions of CTAB lead to the formation of ellipsoidal nanostructures, while higher CTAB concentrations favor the generation of nanowires. The concentration of CTAB can be finely adjusted to exert precise shape control of the produced nanoparticles. Furthermore, variations in the concentrations of ethanol, CTAB, and NaOH can introduce further adjustments to the morphology and size of the CuO nanoparticles. The toxicity of CuO nanoparticles is also influenced by their size, shape, and crystal plane. CuO nanoparticles characterized by high surface-to-volume ratios are particularly desirable for achieving enhanced photocatalytic performance. Fig. 2b and c provides a comprehensive visual representation of the stepwise synthesis process of the PVA-coated CuO NPs. In Fig. 2b, the transformation is clearly evident as we follow the progression of the CuO nanoparticle synthesis. Initially, with the addition of $CuSO_4{\cdot}5H_2O$ to the system containing NaOH and CTAB, a striking transition occurs, resulting in the formation of a light blue copper hydroxide suspension (I). Subsequently, upon the introduction of $NaBH_4$, we witness a pronounced color shift, transitioning from the initial light blue to a rich dark brown hue (II). The combination of $NaBH_4$ and H_2 synergistically brings about the reduction of $Cu(OH)_2$ and Cu^{2+}. This process leads to the creation of small copper nanoparticles located at the outer

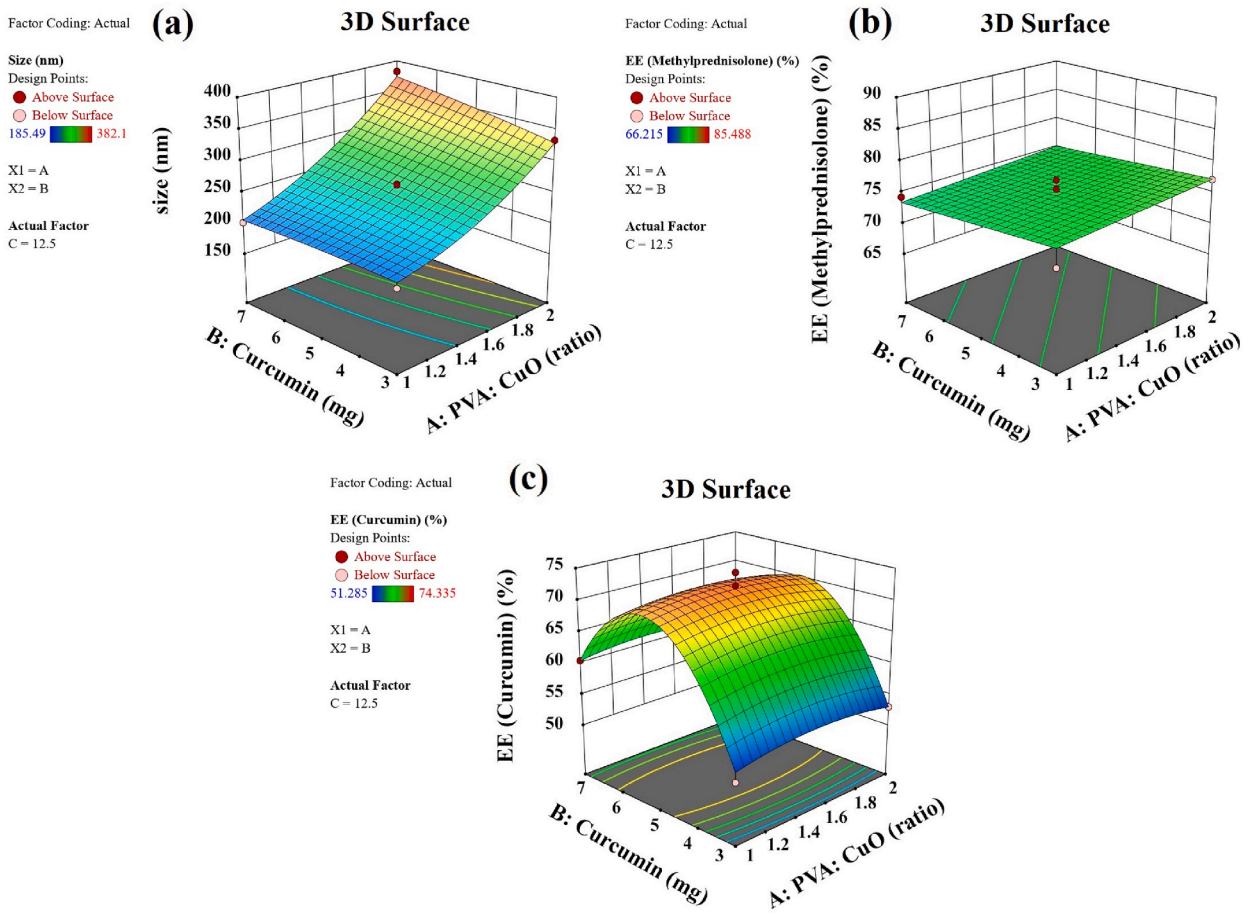

Fig. 1. Three-dimensional response surface plots of PVA-coated CuO NP formulations for a) size, b) EE, and c) EE.

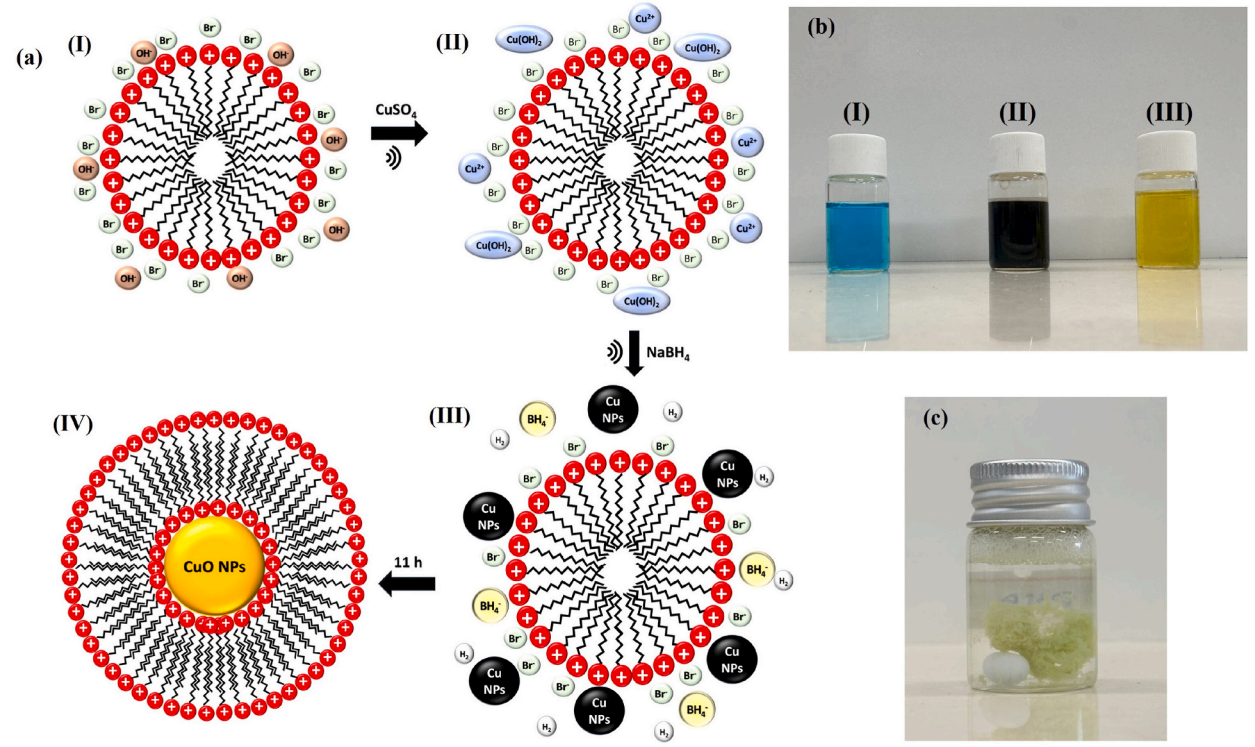

Fig. 2. Illustration depicting the synthesis process of CuO nanoparticles using the sonochemical technique. Stage I: CTAB micelle in an alkaline environment (colorless). Stage II: Suspension of copper hydroxide (pale blue hue). Stage III: Reduction of $Cu(OH)_2$ and Cu^{2+} facilitated by the cooperative influence of $NaBH_4$ and H_2, giving rise to nuclei containing small Cu NPs formed at the micelle's periphery (resulting in a dark brown suspension). Stage IV: Nucleation is achieved through the oxidation of Cu NPs, accompanied by structural rearrangement of the micelle. Subsequently, CTAB micelles encapsulate the newly formed CuO NPs, leading to a colloidal suspension with a yellow appearance. Reprinted from Ref. [22] used under Creative Commons Attribution (CC BY) license (a), visual representation of the stepwise synthesis process of the CuO NPs and its color change (b) and PVA-coated CuO NPs (c).

part of the micelle, which causes the suspension to appear dark brown. Nucleation occurs as Cu NPs oxidize, leading to a rearrangement of the micellar structure. Following this, CTAB micelles encapsulate the newly formed CuO NPs, resulting in a colloidal suspension with a yellow hue (III). As depicted in Fig. 2c, the PVA-coated CuO nanoparticles exhibit a transformative NPs system,

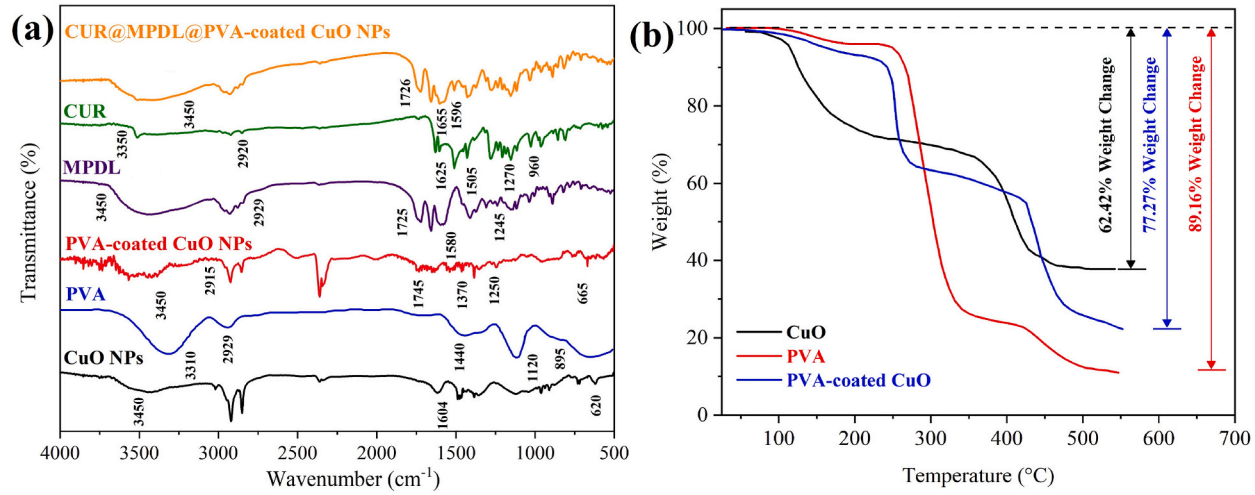

Fig. 3. (a) FTIR analysis of CuO NPs, PVA, PVA-coated CuO NPs, MPDL, CUR, and CUR@MPDL@PVA-coated CuO NPs. CuO NPs, PVA, and PVA-coated CuO NPs spectra offer insights into the chemical composition and surface modifications. (b) Thermogravimetric Analysis (TGA) Curve of CuO, PVA, and PVA-coated CuO NPs.

underlining the successful synthesis and encapsulation of the CuO nanoparticles within the PVA matrix.

3.3. FTIR analysis

The FTIR spectrum of CuO nanoparticles shows Cu-O bond stretching (500-700 cm^{-1}) and O-H stretching/bending (3250-3600 cm^{-1}, 1560-1660 cm^{-1}) (Fig. 3a). PVA is identified by its peaks at 3310 cm^{-1} (O-H stretch), 2929 cm^{-1} (C-H stretch), 1440 cm^{-1} (CH_2 and CH_3 deformation and O-H bend), 1050-1210 cm^{-1} (C-O-C stretch), and 840-900 cm^{-1} (C-H bend). PVA-coated CuO nanoparticles exhibit peaks for O-H (3500-3300 cm^{-1}), C-H (3000-2810 cm^{-1}), C=O (1750-1725 cm^{-1}), C-O (1300-1100 cm^{-1}), and aliphatic C-H bending (1460-1360 cm^{-1}), with CuO metal-oxygen stretching (650-400 cm^{-1}). Methylprednisolone (MPDL) features include hydroxyl (-OH) stretching (3310-3550 cm^{-1}), carbonyl (C=O) stretching (1650-1750 cm^{-1}), aliphatic C-H stretching (2830-3000 cm^{-1}), aromatic C=C stretching (1500-1600 cm^{-1}), and ether C-O stretching (1000-1300 cm^{-1}). Curcumin (CUR) shows O-H groups (3200-3500 cm^{-1}), aliphatic/aromatic C-H stretching (3000-2800 cm^{-1}), carbonyl (C=O) stretching (1600-1630 cm^{-1}), aromatic C=C stretching (1505 cm^{-1}), ether/phenolic stretching (1210-1330 cm^{-1}), and aromatic/aliphatic C-H bending (1000-900 cm^{-1}, 1450-1350 cm^{-1}) [24]. CUR@MPDL@PVA-coated CuO nanoparticles combine these features, with distinctive peaks for methylprednisolone (1726 cm^{-1} for C=O, 1607 cm^{-1} for C=C) and curcumin (1655 cm^{-1} for C=O, 1596 cm^{-1} for C=C) alongside PVA and CuO indicators.

3.4. TGA analysis

The TGA curve of CuO typically displays an initial weight loss, transpiring in the temperature range of 80–130 °C, which was attributed to eliminating physically adsorbed water in the sample (Fig. 3b). The most significant weight loss occurs between 200 °C and 400 °C. This stage is typically attributed to organic residues that may have been present from the synthesis process. CuO nanoparticles can have adsorbed water or other volatile organic materials on their surface, which would decompose or evaporate within this temperature range. After this significant decomposition phase, the weight stabilizes beyond 400 °C, suggesting that the material has reached a thermally stable phase. CuO nanoparticles maintain structural integrity in this higher temperature range, as no further significant weight loss is observed. This stability is consistent with the behavior of metal oxides, which generally have high thermal resistance and are less prone to decomposition at elevated temperatures. The analysis confirms that the weight-loss stages are primarily due to the elimination of surface-bound species rather than the decomposition of CuO, which remains stable at temperatures higher than 400 °C [25]. TGA curve of PVA demonstrates sequential weight loss steps at specific temperature ranges: an initial moisture loss at lower temperatures (50–100 °C), followed by significant degradation steps between 200-350 °C and 350–450 °C, representing PVA decomposition, and finally, a stage at higher temperatures (450–600 °C) indicating the formation of char residues [26]. TGA curve of PVA-coated CuO NPs exhibits distinct weight loss steps at specific temperature ranges: an initial moisture loss and PVA degradation

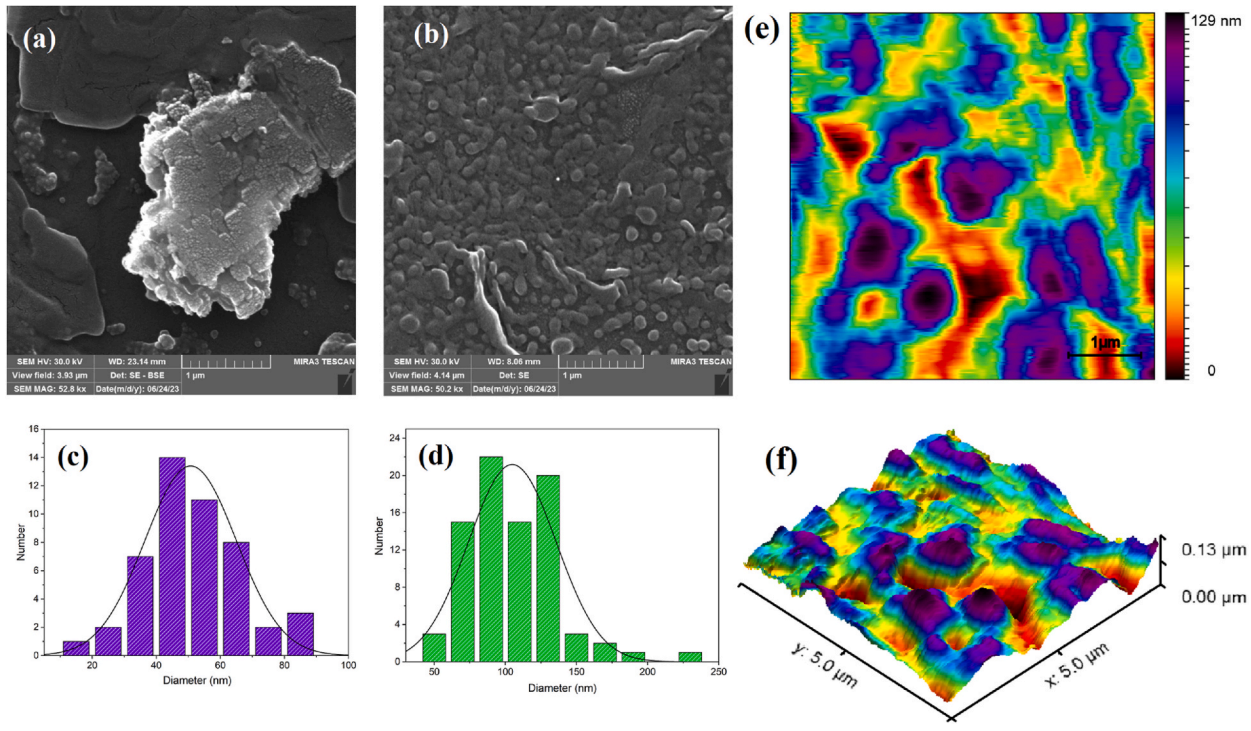

Fig. 4. (a–d) FESEM Images and Size Distribution Analysis of CuO NPs and PVA-coated CuO NPs. 2D (e) and 3D (f) AFM images of PVA-coated CuO NPs.

between 50 and 100 °C, followed by significant decomposition of PVA and CuO oxidation in the range of 200–350 °C, and finally, a char formation stage at higher temperatures (350–600 °C) indicating the presence of residual components or stable residues in the NPs.

3.5. Field Emission Scanning Electron Microscopy (FESEM) images

Fig. 4 presents the FESEM images of the CuO NPs and PVA-coated CuO NPs. In Fig. 4a–d, the uniform size distribution is exhibited by both the CuO NPs and the PVA-coated CuO NPs. This uniformity is an essential indicator of a well-controlled synthesis process. The uniform size distribution seen in both sets of nanoparticles confirms the successful synthesis of CuO NPs and their subsequent coating with PVA. The use of ImageJ software for particle size analysis is a common and reliable technique in materials science. The analysis reveals that CuO NPs have an average size of approximately 50.7 nm, whereas PVA-coated CuO NPs are slightly larger, with an average size of about 104.8 nm. This size difference is noteworthy and could be attributed to the presence of the PVA coating. The increase in the average size of PVA-coated CuO NPs compared to uncoated CuO NPs (from 50.7 nm to 104.8 nm) is a direct consequence of the PVA coating.

3.6. Atomic force microscopy (AFM) analysis

In Fig. 4e and f, the PVA-coated CuO nanoparticles exhibit an average size of approximately 450 nm. This size measurement represents the lateral dimensions of the nanoparticles as imaged by AFM. This observed size increase compared to the uncoated CuO nanoparticles underscores the significant impact of the PVA coating on their dimensions. The increase in size of the nanoparticles is directly attributed to the presence of the PVA coating. When nanoparticles are coated with a polymer like PVA, an additional layer around the nanoparticles is introduced, leading to an increase in their overall size. This increase is often desirable for certain applications, as it can influence properties such as colloidal stability, drug loading capacity, and surface functionalization.

3.7. Dynamic-light scattering (DLS) analysis

Fig. 5a illustrates the particle size distribution of CuO NPs (a), PVA-coated CuO NPs (b), and CUR@MPDL@PVA-coated CuO NPs. The uncoated copper oxide nanoparticles (CuO) have an average size of approximately 200 nm. Modification with PVA appears to slightly reduce the particle size, suggesting successful coating of the nanoparticles [27]. However, the most notable change in size is observed with the CUR@MPDL@PVA-Coated CuO formulation, which presents an average size of around 225 nm. The addition of CUR and MPDL to the PVA-coated CuO results in a larger NP ($p < 0.05$). This size augmentation may be attributed to the combined loading of CUR and MPDL onto the PVA-coated nanoparticles, which could impact the therapeutic efficacy and delivery of the drugs

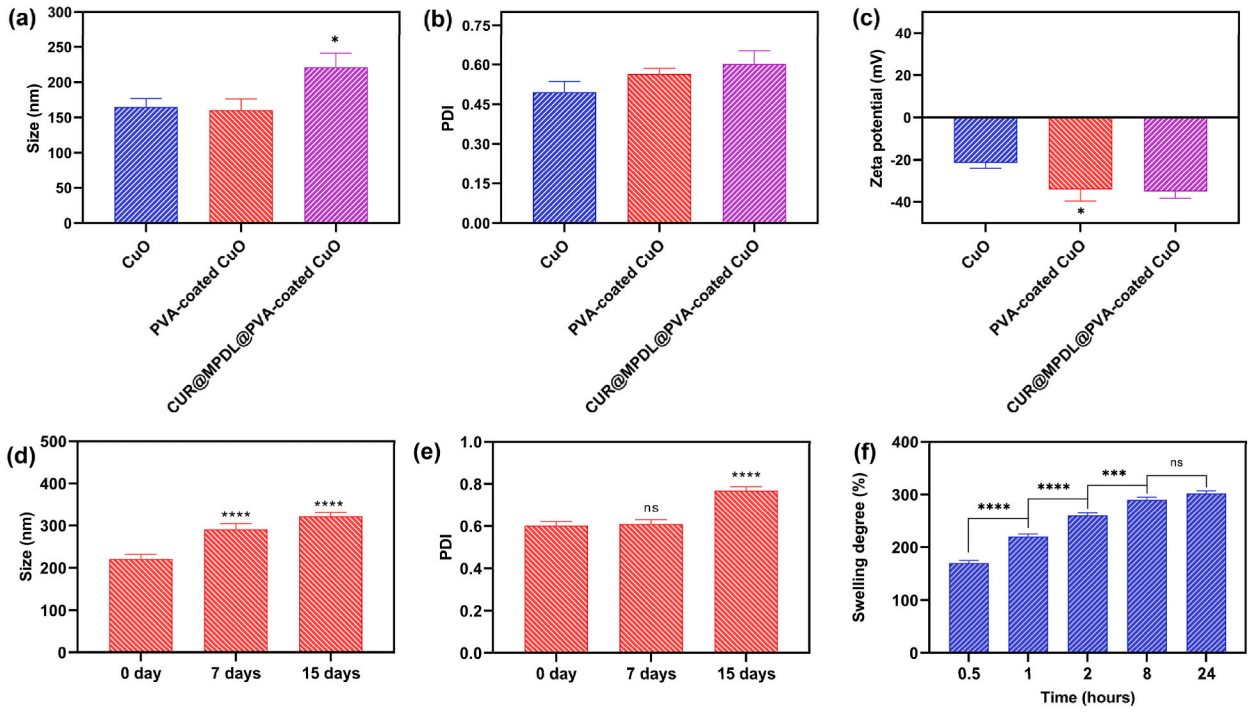

Fig. 5. (a–c) size, PDI, and zeta potential analysis of CuO NPs, PVA-coated CuO NPs, and CUR@MPDL@PVA-coated CuO NPs, (d,e) size and PDI stability evaluation of PVA-coated CuO NPs, and (f) swelling behavior of PVA-coated CuO NPs after 24 h.

encapsulated within the nanoparticle system. The zeta potential analysis conducted on CuO, PVA-coated CuO, and CUR@MPDL@PVA-coated CuO demonstrates a negative surface charge across all NPs, with values ranging from approximately −20 mV to −40 mV (Fig. 5c). The PVA-coated CuO nanoparticles exhibited a significantly lower zeta potential compared to the uncoated CuO, suggesting enhanced colloidal stability due to the surface modification. Furthermore, the CUR@MPDL@PVA-coated CuO nanoparticles showed a comparable decrease in zeta potential to the PVA-coated CuO, implying that the drug loading process did not negatively impact the colloidal stability of the nanoparticles. The substantial negative zeta potential suggests that the CUR@MPDL@PVA-coated CuO nanoparticles might exhibit enhanced circulation times *in vivo*, which is beneficial for drug delivery applications [28]. The polydispersity index (PDI) data illustrates the size distribution uniformity of the CuO nanoparticles, both uncoated and coated with polyvinyl alcohol (PVA), as well as the drug-loaded CUR@MPDL@PVA-coated CuO nanoparticles (Fig. 5b). Our results demonstrate that all nanoparticle formulations maintained a PDI below 0.7, suggesting a moderately uniform size distribution with no significant difference among the groups. The PDI for the CuO nanoparticles was observed at approximately 0.45, while the PVA-coated CuO and the drug-loaded CUR@MPDL@PVA-coated CuO both presented slightly higher values, yet still indicating a relatively homogeneous particle size distribution. PVA-coated CuO NPs were tested for their physical stability by comparing their size before and after 15 days of storage. As shown in Fig. 5d and e, the particle size shows a moderate increase from 0 days to 7 and 15 days. The initial size is around 160 nm, and it increases slightly to about 198 nm after seven days and further to approximately 264 nm after 15 days. However, this increase is not excessive, with size stabilizing after an initial period, suggesting that the particles maintain a stable size without significant aggregation over time. The increase in size over time is expected in nanoparticle systems due to minor swelling or surface modifications. For the PDI stability, the values show no significant change between day 0 and days 7 or 15. This consistency in PDI values supports the hypothesis that the particles maintain a relatively uniform size distribution throughout the stability assessment period. A stable PDI value implies that the nanoparticles are not only resisting aggregation but also maintaining a homogeneous dispersion, which is crucial for their effectiveness in biological applications.

3.8. Swelling behavior of PVA-coated CuO NPs

The swelling degree of the PVA-coated CuO NPs observed over 24 h at pH = 7 displayed dynamic behavior (Fig. 5f). Initially, at 30 min, the swelling degree was measured at 170 %, indicating the material's ability to absorb and retain water. Over the subsequent hours, the swelling continued to increase, reaching 220 % at 1 h and 260 % at 2 h, reflecting a progressive absorption of moisture. After 8 h, the swelling degree peaked at 290 %, suggesting that the NPs had absorbed a substantial amount of water. Interestingly, after 24 h, the swelling degree reached 302 %, indicating a possible saturation point or equilibrium in the swelling process [29,30]. The role of PVA in these NPs is crucial. PVA is known for its water-soluble and hydrophilic properties. PVA's hydrophilic nature makes it capable of absorbing and retaining water. This property enhances the NPs's water-absorbing capacity, which is evident in the swelling behavior observed over time.

3.9. Drug loading and release study

In this study, the drug release behavior of PVA-coated CuO NPs was investigated, aiming to elucidate their potential as a drug

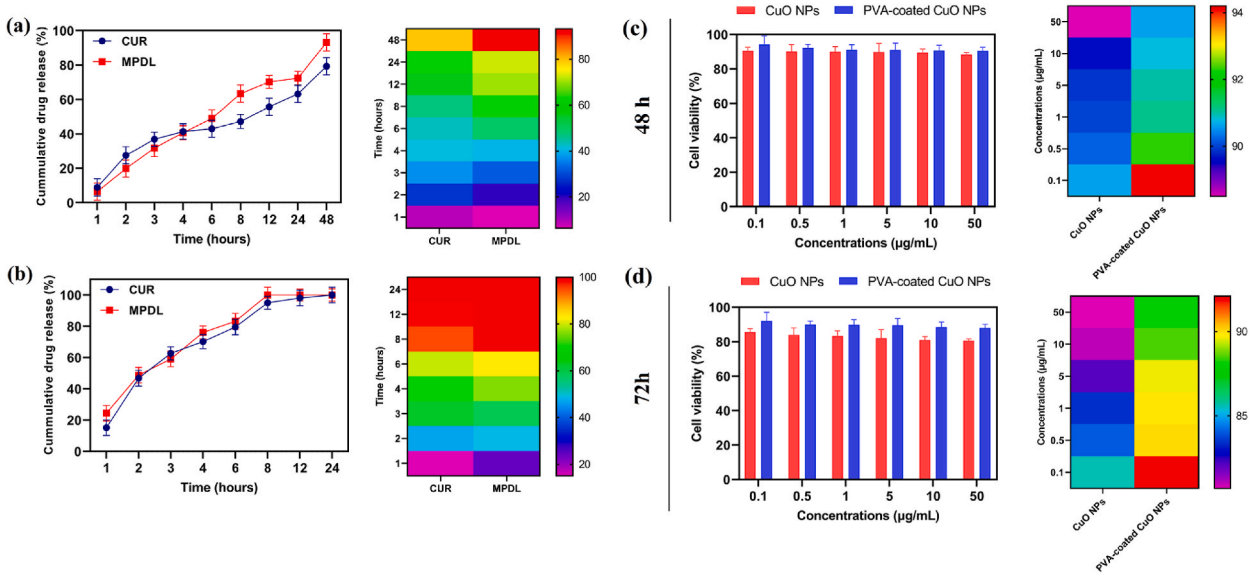

Fig. 6. (a–b) Drug release profile of CUR and MPDL from PVA-coated CuO NPs (a) and PVA matrix (b). (c–d) MTT Assay of CuO NPs and PVA-coated CuO NPs on Fibroblast Cells after 48 and 72 h.

delivery system (Fig. 6a and b). Specifically, the relationship between the encapsulation and subsequent release of CUR and MPDL within the NP matrix was examined under physiological conditions (pH 7.4). During the initial drug-loading step, intriguing insights were provided into the interaction of drug molecules with the NPs. Comparatively, a higher propensity for drug incorporation was observed in the pure PVA matrix (90.86 %). This phenomenon was attributed to the expansive nature of the pure PVA matrix, which readily allowed drug molecules to permeate the matrix and establish interactions with the polymeric chains. In contrast, the presence of CuO nanoparticles in the NPs exerted a noticeable influence on the drug-loading process (82.10 %). The attractive forces between CuO nanoparticles and the polymer chains contributed to the contraction of the matrix, thus impeding the water uptake process. This behavior aligned with the principles of reduced water absorption in the presence of nanoparticles, as previously reported [33,38]. To comprehensively assess the drug release profiles, the release of curcumin and methylprednisolone from both NPs and pure PVA was monitored under pH 7.4 conditions over 48 h. A significantly higher release of the encapsulated drugs was observed in the pure PVA compared to the NPs, with 79.4 % and 93.17 % release for CUR and MPDL from the composite after 48 h, in contrast to 100 % release for CUR and MPDL from the PVA matrix after 24 and 8 h, respectively. The reduced drug release from the NPs could be attributed to the hindrance imposed by the presence of CuO nanoparticles. Specifically, the entrapped drug molecules faced hindered diffusion within the contracted network. Table 2 provides the results of a kinetic study for CUR and MPDL release from PVA-coated CuO NPs and PVA matrix. Various kinetic models were applied to analyze the release behavior, and the determination coefficient (R^2) and the release exponent (n) for the Korsmeyer-Peppas model are presented for each sample. The Korsmeyer-Peppas model, as indicated by its R^2 values, appears to be a good fit for the data, suggesting a non-Fickian release mechanism for these drug-loaded systems. The release exponent values further characterize the release mechanism, with values around 0.5 indicating Fickian diffusion and values above 0.5 suggesting anomalous or non-Fickian diffusion.

3.10. MTT assay

The MTT assay is a widely used colorimetric assay employed to assess the metabolic activity of living cells [31]. In this context, the study aimed to investigate the cytotoxic effects of CuO NPs and PVA-coated CuO NPs on Human Foreskin Fibroblasts (HFF-1) cells. The research findings, as presented in Fig. 6c and d, indicate that the CuO NPs and PVA-coated CuO NPs did not exhibit significant cytotoxic effects on HFF-1 cells, even at relatively high concentrations (up to 50 μg/mL) following 72 h of exposure. The observed cell viability ranged from approximately 90 %–88.5 % and 94.2 %–90.6 % across the concentration range of 0.1–50 μg/mL after 48 h for CuO NPs and PVA-coated CuO NPs, suggesting that the nanocarrier formulation did not adversely impact the fibroblast cells. Additionally, the CuO NPs and PVA-coated CuO NPs displayed consistent cell viability levels across all tested concentrations, with values spanning from 85.6 % to 80.7 % and 92.1 %–88.1 % after 72 h for CuO NPs and PVA-coated CuO NPs.

3.11. Hemocompatibility test

In order to use materials in the biomedical field, it is imperative that their biocompatibility be evaluated. Cheng et al. suggest that the hemolytic activity test is a dependable and scientific approach to assessing a synthetic material's biocompatibility with living systems [32]. Hemostasis in nanoparticles is frequently disregarded, even though most of them come into contact with blood during their journey through the body. Red blood cells (RBCs) may become hemolyzed as a result of breaking their cell membrane, which is caused by these particles altering the shape of RBCs. Because these detrimental interactions between nanoparticles and the bloodstream stimulate the immune system to suppress, they can increase the risk of infection, malignancy, and inflammatory and autoimmune diseases [33]. In this study, CUR@MPDL@PVA-coated CuO NPs were investigated for blood compatibility (Fig. 7). All CUR@MPDL@PVA-coated CuO NPs concentrations (1800, 1600, 1400, 1200, 1000, and 800 μg mL^{-1}) showed hemolysis percentages less than 5 %, which can be regarded as safe NPs [34]. The presence of PVA in the nanoformulation may have contributed to the safe hemolysis of human erythrocytes by facilitating NPs' escape from the reticuloendothelial system and inhibiting macrophage scavenging.

3.12. Therapeutic efficacy of CUR@MPDL@PVA-coated CuO NPs in CFA-induced arthritis model

Adjuvant immunized arthritis (AIA) rat was conducted to assess the effectiveness of CUR@MPDL@PVA-coated CuO NPs and other compounds in real-time. In this study, from day 9 to day 27, different treatments were administered to rats: saline, CUR, MPDL, and CUR@MPDL@PVA-coated CuO NPs, with the saline-only group serving as a control. Paw swelling is a crucial measure for assessing anti-inflammatory effects. The saline group exhibited a steady increase in paw swelling throughout the experiment up to day 28. CUR

Table 2
Kinetic study of CUR and MPDL from PVA-coated CuO NPs and PVA matrix.

Sample	Zero order	First order	Higuchi	Korsmeyer-peppas	
	R^2	R^2	R^2	R^2	n
PVA-coated CuO NPs (CUR)	0.7535	0.9223	0.8843	0.795	0.4626
PVA-coated CuO NPs (MPDL)	0.6795	0.929	0.8441	0.8154	0.6154
PVA (CUR)	0.5378	0.854	0.7294	0.7589	0.5391
PVA (MPDL)	0.5233	0.6522	0.7182	0.8245	0.4376

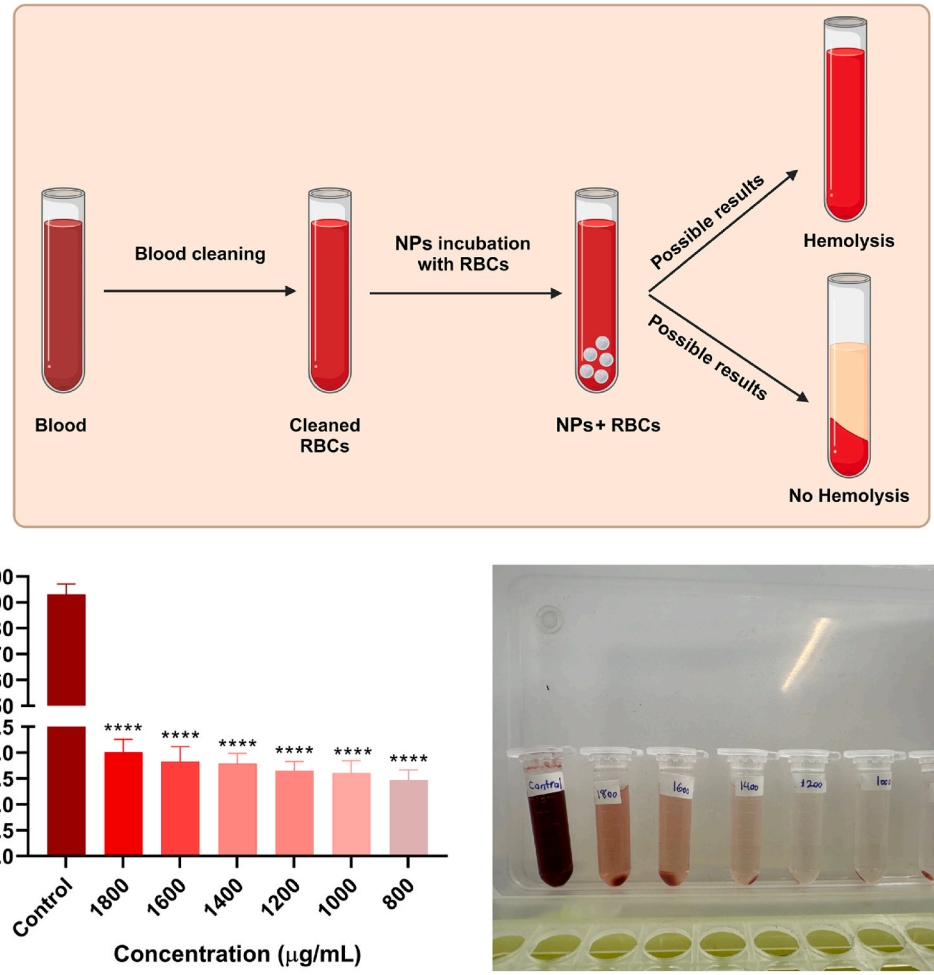

Fig. 7. At different concentrations, the hemolysis percentage of CUR@MPDL@PVA-coated CuO NPs nanoformulation was assessed in relation to a positive control (SDS: sodium dodecyl sulfate). Human volunteers in good health provided fresh whole blood samples, which were then subjected to varying concentrations (1800, 1600, 1400, 1200, 1000, and 800 μg mL^{-1}) of CUR@MPDL@PVA-coated CuO NPs.

and free MPDL showed some impact on reducing paw swelling compared to the control, but they did not significantly reduce swelling beyond the levels observed on day 8. CUR@MPDL@PVA-coated CuO NPs markedly reduced paw swelling compared to the CUR and free MPDL groups, demonstrating the effectiveness of nanocarrier systems (Fig. 8c and d). Notably, CUR@MPDL@PVA-coated CuO NPs were most effective, significantly reducing paw swelling to almost the initial levels observed on day 1, showing its superior anti-inflammatory properties. The final paw volume measured on day 28 reflected the impact of each treatment. Additionally, the mean clinical scores of rats in each group were calculated (Fig. 8a). The average clinical score for saline-treated AIA rats was 4.5, free CUR was 4.2, and free MPDL was 3.8, indicating minimal effectiveness in improving conditions. However, CUR@MPDL@PVA-coated CuO NPs showed a significant reduction in clinical scores compared to control and free treatments, highlighting the potential of these formulations.

3.13. Pro-inflammatory cytokine expression in serum

Regarding pro-inflammatory cytokine expression in serum, it is well-established that cytokines like TNF-α and IL-1β are linked to inflammation in rheumatoid arthritis. This study measured these cytokines in the serum of AIA rats (Fig. 8b). Elevated levels of pro-inflammatory cytokines were found in the model rats compared to normal ones. There was no significant difference in cytokine levels between the CUR and MPDL-treated groups and the AIA model. However, CUR@MPDL@PVA-coated CuO NPs demonstrated significantly lower TNF-α and IL-1β levels than the AIA model and free treatment groups. This suggests that the enhanced penetration of CUR@MPDL@PVA-coated CuO NPs into synovial tissues may effectively reduce pro-inflammatory cytokine expression. It has been observed that inflammation in rheumatoid arthritis joints leads to the formation of gaps approximately 500–700 nm wide in the neighboring endothelial cells.

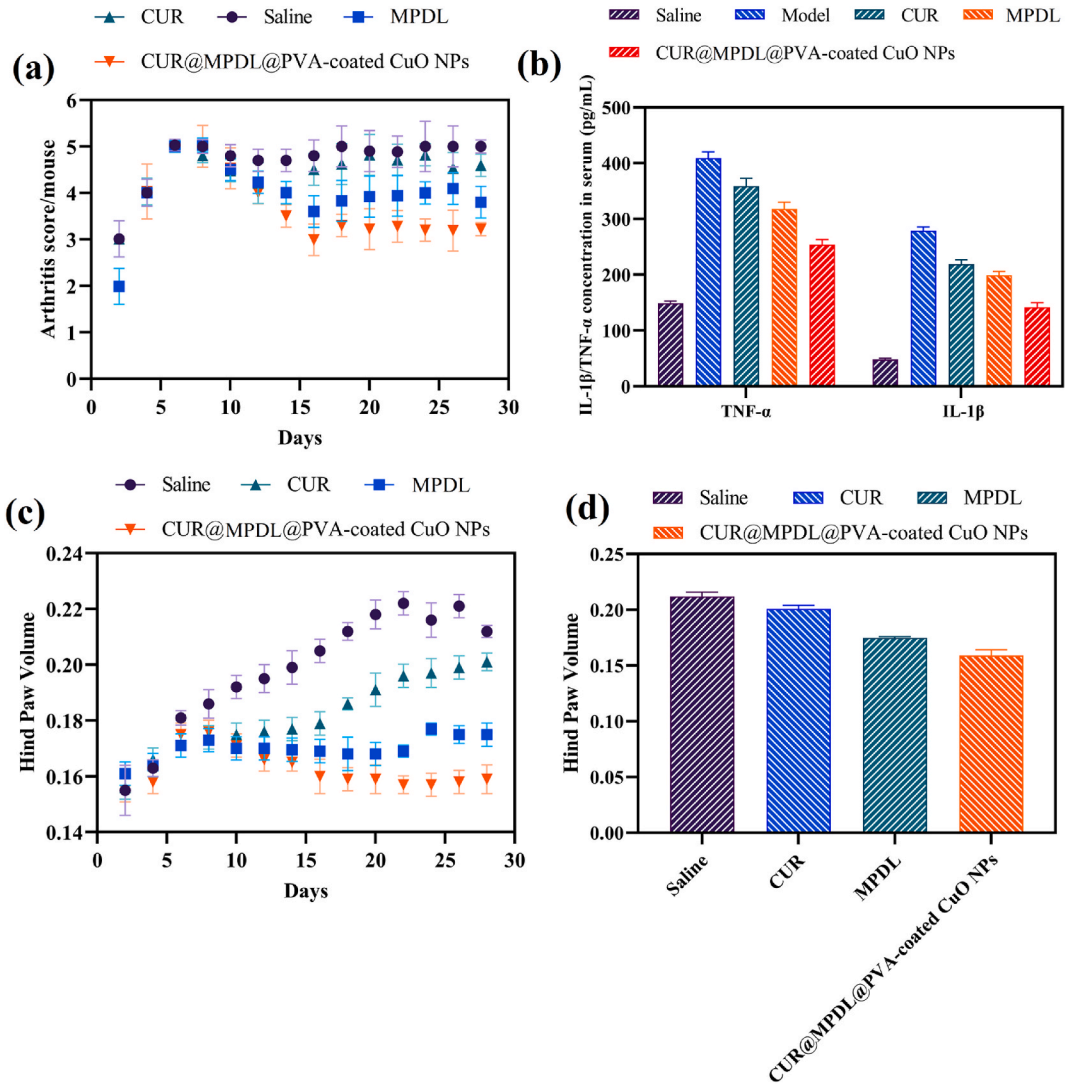

Fig. 8. (a) Concentrations of proinflammatory cytokines (TNF-α and IL-1β) in the serum of rats with arthritis measured on day 28, (b) amounts of proinflammatory cytokines (TNF-α and IL-1β) in the serum of AIA rats, (c–d) average clinical scores observed in experimental rats after receiving specific treatments.

4. Discussion

The PVA layer adds an extra thickness and contributes to the overall size of the nanoparticles. This information is crucial, especially in applications where the size of nanoparticles plays a significant role in their behavior, such as drug delivery, where particle size can affect drug release kinetics and cellular uptake. According to previous studies, CuO and CuO-coated PVA particles have spherical shapes [35–37]. CuO nanoparticles typically have a size between 19 and 49 nm. [35], 40–70 nm [36], and about 50–70 nm [37]. Swelling properties of pure PVA matrix were enhanced by the incorporation of CuO into the structure [38]. The SEM images of CuO nanoparticles calcined at different temperatures show poly-dispersive and spherically shaped NPs. The SEM images of CuO/PVA NPs show that the addition of PVA to CuO nanoparticles does not significantly alter the morphology of CuO nanoparticles. However, the surfactant coating on CuO nanoparticles enhances their thermophysical properties [39]. The SEM images of PVA/CuO/Gr- NPs show that the CuO nanoparticles are well dispersed in the PVA matrix [40]. The controlled size increment within the nano-range suggests the potential for enhanced cellular uptake and retention at the target site, which is critical for the treatment of conditions such as rheumatoid arthritis. Bin Mobarak et al. reported that the particle size of synthesized CuO NPs was 273 nm [41]. The average hydrodynamic diameter and the polydispersity index (PDI) of CuO-NPs@H-PLGA/PDA/PEG NS were 288 nm and 0.201, respectively, while for the CuO-NPs@L-PLGA/PDA/PEG NS they were found to be 257 nm and 0.143, respectively. They reported that the size of CuO-loaded PLGA nanospheres increased compared to those of uncoated nanospheres due to the higher hydrophilic nature of PDA and PEG [42]. PVA acts as a sponge, absorbing water and causing the NPs to swell as it takes in moisture from its surroundings. The coating

of CuO NPs by PVA can be advantageous for drug delivery applications by providing a means to tailor the release of pharmaceutical agents. The swelling properties of the prepared NPs were investigated by Ahamadian et al., where the swelling ratio of the PVA/CuO NPs was around 300–500 (%) [43]. In another study, it was demonstrated that the swelling properties of pure PVA hydrogel were enhanced with the addition of CuO to the hydrogel structure. The swelling degree of PVA/CuO NPs hydrogel reached a maximum value of around 570 % [44]. Banihashem et al. reported that cisplatin-loaded thiolated gold@CS-g-PNVCL NFs exhibited minimal cytotoxicity in HMF3A cells [45]. The results from the MTT assay provide substantial evidence that the CuO NPs and PVA-coated CuO NPs have low cytotoxicity, rendering them a promising candidate for various drug delivery applications. Our developed NPs, being around 300 nm, can effectively reach these inflamed areas through a distinctive process known as the ELVIS (extravasation via leaky vasculature and inflammatory cell-mediated sequestration) effect. This mechanism underlines the remarkable anti-inflammatory capabilities of our formulations. Li et al. utilized AIA rats to study the efficacy of Folate-conjugated dexamethasone/siRNA-loaded polymeric micelles and other formulations in real time [46,47]. For this purpose, between days 9 and 27, rats were treated with saline, naked siRNA, dexamethasone, dexamethasone/siRNA-loaded polymeric micelles, and Folate-conjugated dexamethasone/siRNA-loaded polymeric micelles, respectively. Folate-conjugated dexamethasone/siRNA-loaded polymeric micelles exhibited the greatest decrease in the paw volume, almost flattening the degree of paw volume as that of the original paw volume on day 1indicating a superior anti-inflammatory activity. Similarly, clinical scores of DS-PM and DS-FPM showed a significant decrease compared to control and free groups, indicating the potential of the micellar formulations. Also, Aslam et al. studied the anti-arthritic activity of CUR and meloxicam (MLX) co-loaded PLGA NPs (n) in adjuvant-induced arthritic rats [47]. The treatment of arthritic rats with CUR, MLX, CUR plus MLX, nCUR, nMLX, and nCur/MLX demonstrated a gradual reduction in these parameters from day 7 onwards in comparison to the model group ($p \leq 0.05$). Furthermore, a notable improvement in reducing paw swelling and arthritic score was observed in nCur, nMlx, and nCur/Mlx-treated groups compared to the pure compound-treated groups; however, nCur/Mlx showed the highest attenuating effects among all treatments. In this study, saline treatment of AIA rats resulted in an average clinical score of 4.5, free CUR of 4.2, and free MPDL of 3.8, suggesting only modest improvement in conditions. However, in contrast to free and control treatments, CUR@MPDL@PVA-coated CuO NPs demonstrated a noteworthy decline in clinical scores, underscoring the potential of these formulations compared to previous studies.

5. Conclusion

In this study, PVA-coated CuO NPs were synthesized by dispersing CuO nanoparticles into a PVA solution. The average size of both the CuO nanoparticles and the PVA-coated CuO NPs was determined to be 50.7 nm and 104.8 nm, respectively. The results indicated that these NPs possess distinctive characteristics suitable for biomedical applications, notably an exceptional swelling capacity of up to 302 %. The drug loading capacity of the PVA-coated CuO NPs was quantified, revealing a maximum drug content of 82.10 % in the NPs. PVA-coated CuO NPs exhibited outstanding biocompatibility, as evidenced by cell viability ranging from 88.1 % to 92.1 % at concentrations of 0.1 μg/mL and 50 μg/mL after 72 h, as confirmed by the MTT assay. The PVA-coated CuO nanoparticles exhibited the greatest decrease in hind paw swelling and the lowest clinical scores compared to all other treatment groups, indicating superior anti-inflammatory properties.

The main limitations in this study are related to the use of Freund's Complete Adjuvant (CFA) induced arthritic rat model, which, while useful, might not accurately represent rheumatoid arthritis in humans. It is recommended that more advanced animal models or human-like models with characteristics resembling rheumatoid arthritis in humans be used for future research. Furthermore, the results might not directly apply to clinical trials involving humans. The study only evaluated the short-term therapeutic use of PVA-coated CuO nanoparticles. Long-term studies are required in order to assess the effectiveness of nanoparticles in long-term therapeutic administration without causing possible negative impacts on the other organs. To improve therapeutic efficacy and reduce toxicity, additional research should be conducted to better understand drug release mechanisms and their effect on the immune system. Finally, to make the results more indicative and statistically significant and to further clarify the therapeutic potential of these nanoparticles, larger sample sizes should be used in subsequent studies.

CRediT authorship contribution statement

Kimiya Zarei: Writing – review & editing, Writing – original draft, Supervision, Investigation. **Mehdi Jahanbakhshi:** Writing – original draft, Conceptualization. **Reza Nahavandi:** Visualization, Methodology, Data curation. **Reza Emadi:** Writing – review & editing, Resources, Funding acquisition.

Ethics statement

All procedures used in the present research were approved by the Animal Ethics and Research Committee. The ethical confirmation code is IR.IAU.SRB.REC.1394.433.

Data availability

Data will be made available on request.

Declaration of competing interest

The authors declare that they have no known competing financial interests or personal relationships that could have appeared to influence the work reported in this paper.

References

[1] A.C.o.R.S.o.R.A. Guidelines, Guidelines for the management of rheumatoid arthritis: 2002 update, Arthritis Rheum. 46 (2) (2002) 328–346.
[2] J.S. Smolen, R. Landewé, J. Bijlsma, G. Burmester, K. Chatzidionysiou, M. Dougados, J. Nam, S. Ramiro, M. Voshaar, R. Van Vollenhoven, EULAR recommendations for the management of rheumatoid arthritis with synthetic and biological disease-modifying antirheumatic drugs: 2016 update, Ann. Rheum. Dis. 76 (6) (2017) 960–977.
[3] L.A. Saketkoo, T. Frech, C. Varjú, R. Domsic, J. Farrell, J.K. Gordon, C. Mihai, N. Sandorfi, L. Shapiro, J. Poole, A comprehensive framework for navigating patient care in systemic sclerosis: a global response to the need for improving the practice of diagnostic and preventive strategies in SSc, Best Pract. Res. Clin. Rheumatol. 35 (3) (2021) 101707.
[4] A.-F. Radu, S.G. Bungau, Management of rheumatoid arthritis: an overview, Cells 10 (11) (2021) 2857.
[5] M. Jari, R. Shiari, O. Salehpour, K. Rahmani, Epidemiological and advanced therapeutic approaches to treatment of uveitis in pediatric rheumatic diseases: a systematic review and meta-analysis, Orphanet J. Rare Dis. 15 (1) (2020) 1–12.
[6] H. Liu, Y. Yang, Y. Liu, J. Pan, J. Wang, F. Man, W. Zhang, G. Liu, Melanin-like nanomaterials for advanced biomedical applications: a versatile platform with extraordinary promise, Adv. Sci. 7 (7) (2020) 1903129.
[7] B. Farasati Far, A.A. Isfahani, E. Nasiriyan, A. Pourmolaei, G. Mahmoudvand, A. Karimi Rouzbahani, M. Namiq Amin, M.R. Naimi-Jamal, An updated review on advances in hydrogel-based nanoparticles for liver cancer treatment, Livers 3 (2) (2023) 161–189.
[8] B. Farasati Far, M.R. Naimi-Jamal, M. Sedaghat, A. Hoseini, N. Mohammadi, M. Bodaghi, Combinational system of lipid-based nanocarriers and biodegradable polymers for wound healing: an updated review, J. Funct. Biomater. 14 (2) (2023) 115.
[9] V.W. Xu, M.Z.I. Nizami, I.X. Yin, O.Y. Yu, C.Y.K. Lung, C.H. Chu, Application of copper nanoparticles in dentistry, Nanomaterials 12 (5) (2022) 805.
[10] O. Veiseh, J.W. Gunn, M. Zhang, Design and fabrication of magnetic nanoparticles for targeted drug delivery and imaging, Adv. Drug Deliv. Rev. 62 (3) (2010) 284–304.
[11] Z. Sun, C. Song, C. Wang, Y. Hu, J. Wu, Hydrogel-based controlled drug delivery for cancer treatment: a review, Mol. Pharm. 17 (2) (2019) 373–391.
[12] R.D. Al Bostami, W.H. Abuwatfa, G.A. Husseini, Recent advances in nanoparticle-based co-delivery systems for cancer therapy, Nanomaterials 12 (15) (2022) 2672.
[13] B. Farasati Far, M. Jahanbakhshi, L. Jameie, F. Zolfigol, P. Taromi, Y.N. Ertas, Chitosan-graft-Pomegranate extract hydrogel: a dual-functional pad for antibacterial and antioxidant enhancement for shelf life extension in food packaging, ACS Appl. Polym. Mater. 6 (16) (2024) 9545–9558, https://doi.org/10.1021/acsapm.4c01240.
[14] L. Gautam, S.G. Warkar, S.I. Ahmad, R. Kant, M. Jain, A review on carboxylic acid cross-linked polyvinyl alcohol: properties and applications, Polym. Eng. Sci. 62 (2) (2022) 225–246.
[15] B. Farasati Far, M.R. Naimi-Jamal, M. Jahanbakhshi, H. Rostamani, M. Karimi, S. Keihankhadiv, Synthesis and characterization of chitosan/collagen/polycaprolactone hydrogel films with enhanced biocompatibility and hydrophilicity for artificial tendon applications, Int. J. Biol. Macromol. 253 (2023) 127448, https://doi.org/10.1016/j.ijbiomac.2023.127448.
[16] A. Barui, Synthetic Polymeric Gel, Polymeric Gels, Elsevier, 2018, pp. 55–90.
[17] M. Jahanbakhshi, M. Shahrousvand, Stimuli-Responsive Polymers as Smart Drug Delivery Systems, Modeling and Control of Drug Delivery Systems, Elsevier, 2021, pp. 67–77.
[18] S. Hosseini, M. Shahrousvand, J. Mohammadi-Rovshandeh, M. Jahanbakhshi, A. Javadi, M. Soleimani, H. Jalalian, M. Hajikhani, Fabrication of pH-responsive amphiphilic poly(vinyl alcohol–methyl methacrylate) copolymer nanoparticles for application in cancer drug delivery systems, Iran. J. Sci. Technol. 48 (1) (2024) 99–111, https://doi.org/10.1007/s40995-023-01573-w.
[19] E.A. Kamoun, X. Chen, M.S.M. Eldin, E.-R.S. Kenawy, Crosslinked poly (vinyl alcohol) hydrogels for wound dressing applications: a review of remarkably blended polymers, Arab. J. Chem. 8 (1) (2015) 1–14.
[20] N. Muniyappan, M. Pandeeswaran, A. Amalraj, Green synthesis of gold nanoparticles using Curcuma pseudomontana isolated curcumin: its characterization, antimicrobial, antioxidant and anti-inflammatory activities, Environ. Chem. Ecotoxicol. 3 (2021) 117–124.
[21] G.R. Gandhi, G. Jothi, T. Mohana, A.B.S. Vasconcelos, M.M. Montalvão, G. Hariharan, G. Sridharan, P.M. Kumar, R.Q. Gurgel, H.-B. Li, Anti-inflammatory natural products as potential therapeutic agents of rheumatoid arthritis: a systematic review, Phytomedicine 93 (2021) 153766.
[22] N. Silva, S. Ramírez, I. Díaz, A. Garcia, N. Hassan, Easy, quick, and reproducible sonochemical synthesis of CuO nanoparticles, Materials (2019).
[23] R.A. El-Shiekh, S. El-Mekkawy, S.M. Mouneir, A. Hassan, E. Abdel-Sattar, Therapeutic potential of russelioside B as anti-arthritic agent in Freund's adjuvant-induced arthritis in rats, J. Ethnopharmacol. 270 (2021) 113779, https://doi.org/10.1016/j.jep.2021.113779.
[24] S. Bazzazan, K. Moeinabadi-Bidgoli, Z.A. Lalami, S. Bazzazan, M. Mehrarya, F.E. Yeganeh, F. Hejabi, I. Akbarzadeh, H. Noorbazargan, M. Jahanbakhshi, N. Hossein-khannazer, E. Mostafavi, Engineered UIO-66 metal-organic framework for delivery of curcumin against breast cancer cells: an in vitro evaluation, J. Drug Deliv. Sci. Technol. 79 (2023) 104009, https://doi.org/10.1016/j.jddst.2022.104009.
[25] A.S. Prasad, Green synthesis and spectral analysis of surface encapsulated copper (II) oxide nanostructures, Materials Science-Poland 37 (3) (2019) 503–509, https://doi.org/10.2478/msp-2019-0062.
[26] M. Jahanbakhshi, M. Shahrousvand, Preparation and characterization of cross-linked poly (vinyl alcohol-co-methyl methacrylate) colloidal nanoparticles from hydrolysis of poly (vinyl acetate-co-methyl methacrylate) as a promising cancer drug delivery system, Int. J. Polym. Mater. Polym Biomaterials. 73 (4) (2024) 250–265, https://doi.org/10.1080/00914037.2022.2155158.
[27] B. Farasati Far, M.R. Naimi-Jamal, M. Jahanbakhshi, H.T. Mohammed, U.S. Altimari, J. Ansari, Poly (3-thienylboronic acid) coated magnetic nanoparticles as a magnetic solid-phase adsorbent for extraction of methamphetamine from urine samples, J. Dispersion Sci. Technol. (2022) 1–11.
[28] A. Dastneshan, S. Rahiminezhad, M. Naderi Mezajin, H. Nouri Jevinani, I. Akbarzadeh, M. Abdihaji, R. Qahremani, M. Jahanbakhshi, Z. Asghari Lalami, H. Heydari, H. Noorbazargan, E. Mostafavi, Cefazolin encapsulated UIO-66-NH2 nanoparticles enhance the antibacterial activity and biofilm inhibition against drug-resistant S. aureus: in vitro and in vivo studies, Chem. Eng. J. 455 (2023) 140544, https://doi.org/10.1016/j.cej.2022.140544.
[29] B. Farasati Far, M.R. Naimi-Jamal, M. Jahanbakhshi, S. Keihankhadiv, F. Baradarbarjastehbaf, Enhanced methylene blue adsorption using single-walled carbon nanotubes/chitosan-graft-gelatin nanocomposite hydrogels, Sci. Rep. 14 (1) (2024) 19217, https://doi.org/10.1038/s41598-024-69969-1.
[30] B. Farasati Far, M.R. Naimi-Jamal, M. Jahanbakhshi, S.A. Khalafvandi, M. Alian, D. Razeghi Jahromi, Decontamination of Congo red dye from aqueous solution using nanoclay/chitosan-graft-gelatin nanocomposite hydrogel, J. Mol. Liq. 395 (2024) 123839, https://doi.org/10.1016/j.molliq.2023.123839.
[31] B. Farasati Far, M.R. Naimi-Jamal, M. Jahanbakhshi, A. Hadizadeh, S. Dehghan, S. Hadizadeh, Enhanced antibacterial activity of porous chitosan-based hydrogels crosslinked with gelatin and metal ions, Sci. Rep. 14 (1) (2024) 7505, https://doi.org/10.1038/s41598-024-58174-9.
[32] Y. Cheng, B. Farasati Far, M. Jahanbakhshi, S. Bahrami, P. Tamimi, M. Sedaghat, E. Ghazizadeha, Exploring the potential of a polyvinyl alcohol/chitosan-based nanofibrous matrix for erythromycin delivery: fabrication, in vitro and in vivo evaluation, RSC Adv. 13 (27) (2023) 18450–18460, https://doi.org/10.1039/D3RA02987E.
[33] P. Gong, Y. Wang, P. Zhang, Z. Yang, W. Deng, Z. Sun, M. Yang, X. Li, G. Ma, G. Deng, S. Dong, L. Cai, W. Jiang, Immunocyte membrane-coated nanoparticles for cancer immunotherapy, Cancers (2021).

[34] H.F. Li, F.Y. Zhou, L. Li, Y.F. Zheng, Design and development of novel MRI compatible zirconium- ruthenium alloys with ultralow magnetic susceptibility, Sci. Rep. 6 (1) (2016) 24414, https://doi.org/10.1038/srep24414.
[35] A.M. Azharudeen, A. Roy, R. Karthiga, S.A. Prabhu, M.G. Prakash, A.M.I. Badhusha, H. Ali, K.M. Katubi, M.R. Islam, Ultrasensitive and selective electrochemical detection of dopamine based on CuO/PVA nanocomposite-modified GC electrode, Int. J. Photoenergy 2022 (2022) 8755464, https://doi.org/10.1155/2022/8755464.
[36] I.H. Hilal, R.H. Jabbar, A.H. Muslime, W.A. Shakir, Preparation (PMMA/PVA)-copper oxide nanocomposites solar cel, AIP Conf. Proc. 2290 (1) (2020), https://doi.org/10.1063/5.0027846.
[37] N. Wongpisutpaisan, P. Charoonsuk, N. Vittayakorn, W. Pecharapa, Sonochemical synthesis and characterization of copper oxide nanoparticles, Energy Proc. 9 (2011) 404–409, https://doi.org/10.1016/j.egypro.2011.09.044.
[38] Z. Malik Faiza, A. Khattak, A.A. Alahmadi, S.U. Butt, Development and investigation of high performance PVA/NiO and PVA/CuO nanocomposites with improved physical, dielectric and mechanical properties, Materials (2022).
[39] J. Shah, M. Ranjan, K.P. Sooraj, Y. Sonvane, S.K. Gupta, Surfactant prevented growth and enhanced thermophysical properties of CuO nanofluid, J. Mol. Liq. 283 (2019) 550–557, https://doi.org/10.1016/j.molliq.2019.03.127.
[40] G.J. Thangamani, K. Deshmukh, K. Chidambaram, M.B. Ahamed, K.K. Sadasivuni, D. Ponnamma, M. Faisal, N.A. Nambiraj, S.K.K. Pasha, Influence of CuO nanoparticles and graphene nanoplatelets on the sensing behaviour of poly(vinyl alcohol) nanocomposites for the detection of ethanol and propanol vapors, J. Mater. Sci. Mater. Electron. 29 (6) (2018) 5186–5205, https://doi.org/10.1007/s10854-017-8484-z.
[41] M. Bin Mobarak, M.S. Hossain, F. Chowdhury, S. Ahmed, Synthesis and characterization of CuO nanoparticles utilizing waste fish scale and exploitation of XRD peak profile analysis for approximating the structural parameters, Arab. J. Chem. 15 (10) (2022) 104117, https://doi.org/10.1016/j.arabjc.2022.104117.
[42] I. Maor, S. Asadi, S. Korganbayev, D. Dahis, Y. Shamay, E. Schena, H. Azhari, P. Saccomandi, I.S. Weitz, Laser-induced thermal response and controlled release of copper oxide nanoparticles from multifunctional polymeric nanocarriers, Sci. Technol. Adv. Mater. 22 (1) (2021) 218–233, https://doi.org/10.1080/14686996.2021.1883406.
[43] Y. Ahmadian, A. Bakravi, H. Hashemi, H. Namazi, Synthesis of polyvinyl alcohol/CuO nanocomposite hydrogel and its application as drug delivery agent, Polym. Bull. 76 (2019) 1967–1983.
[44] Ç. Karakaya, F. Boran, Polyvinyl alcohol/CuO nanocomposite hydrogels: facile synthesis and long-term stability, Balıkesir Üniv. Fen Bilim. Enst. derg 21 (2) (2019) 512–530, https://doi.org/10.25092/baunfbed.624392.
[45] S. Banihashem, M.N. Nezhati, H.A. Panahia, Synthesis of chitosan-grafted-poly(N-vinylcaprolactam) coated on the thiolated gold nanoparticles surface for controlled release of cisplatin, Carbohydr. Polym. 227 (2020) 115333, https://doi.org/10.1016/j.carbpol.2019.115333.
[46] Y. Li, S. Wei, Y. Sun, S. Zong, Y. Sui, Nanomedicine-based combination of dexamethasone palmitate and MCL-1 siRNA for synergistic therapeutic efficacy against rheumatoid arthritis, Drug Deliv. Transl. Res. 11 (6) (2021) 2520–2529, https://doi.org/10.1007/s13346-021-01037-x.
[47] B. Aslam, A. Hussain, M.N. Faisal, Z.-u.-D. Sindhu, R.U. Khan, I.A. Alhidary, S. Naz, V. Tufarelli, Curcumin Co-encapsulation potentiates anti-arthritic efficacy of meloxicam biodegradable nanoparticles in adjuvant-induced arthritis animal model, Biomedicines (2023).